THE ULTRAVIOLET LUMINOSITY FUNCTION OF GALEX GALAXIES AT PHOTOMETRIC REDSHIFTS BETWEEN 0.07 AND 0.25

TAMÁS BUDAVÁRI¹, ALEX S. SZALAY¹, STÉPHANE CHARLOT^{2,3}, MARK SEIBERT⁴, TED K. WYDER⁴, STÉPHANE ARNOUTS⁵, TOM A. BARLOW⁴, LUCIANA BIANCH¹, YONG-IK BYUN⁶, JOSÉ DONAS⁵, KARL FORSTER⁴, PETER G. FRIEDMAN⁴, TIMOTHY M. HECKMAN¹, PATRICK N. JELINSKY⁷, YOUNG-WOOK LEE⁶, BARRY F. MADORE⁸, ROGER F. MALINA⁵, D. CHRISTOPHER MARTIN⁴, BRUNO MILLIARD⁵, PATRICK MORRISSEY⁴, SUSAN G. NEFF⁹, R. MICHAEL RICH¹⁰, DAVID SCHIMINOVICH¹¹, OSWALD H. W. SIEGMUND⁷, TODD SMALL⁴, MARIE A. TREYER^{4,5}, AND BARRY WELSH⁷

Received: 2004 May 6 Accepted: 2004 June 10

ABSTRACT

We present measurements of the UV galaxy luminosity function and the evolution of luminosity density from GALEX observations matched to the Sloan Digital Sky Survey (SDSS). We analyze galaxies in the Medium Imaging Survey overlapping the SDSS DR1 with a total coverage of 44 deg². Using the combined GALEX+SDSS photometry, we compute photometric redshifts and study the LF in three redshift shells between z = 0.07 and 0.25. The Schechter function fits indicate that the faint-end slope α is consistent with -1.1at all redshifts but the characteristic UV luminosity M^* brightens by 0.2 mag from z = 0.07 to 0.25. In the lowest redshift bin, early and late type galaxies are studied separately and we confirm that red galaxies tend to be brighter and have a shallower slope α than blue ones. The derived luminosity densities are consistent with other GALEX results based on a local spectroscopic sample from 2dF and the evolution follows the trend reported by deeper studies.

Subject headings: ultraviolet: galaxies — surveys — galaxies: luminosity function, evolution

1. INTRODUCTION

In the era of precision cosmology, the star formation history of the universe can be studied accurately as one can detect evolutionary effects in the observables on top of the global expansion. In particular, the restframe ultraviolet luminosity of galaxies has proven to yield a good handle on the star formation rate (Kennicutt 1998). A number of galaxy surveys have probed the history of star formation at different redshifts. While most studies agree on a relatively rapid rise in the star formation rate (SFR) out to redshift of $z \sim 1$, significant uncertainties remain even at lower redshifts (Lilly et al. 1996; Connolly et al. 1997; Cowie et al. 1999; Wilson et al. 2002). The restframe UV continuum of local galaxies is not accessible from the ground. The balloon-borne telescope of the FOCA experiment (Milliard et al. 1992) had been the best window onto the UV sky until last year, when the Galaxy Evolution Explorer (GALEX) satellite was successfully launched to orbit. This paper is one in the first series of luminosity

Electronic address: budavari@jhu.edu

¹ Department of Physics and Astronomy, The Johns Hopkins University, 3701 San Martin Drive, Baltimore, MD 21218, USA

² Max-Planck-Institute für Astrophysik, Karl-Schwarzschild-Strasse 1, 85748 Garching, Germany

³ Institut d'Astrophysique de Paris, CNRS, 98 bis boulevard Arago, F-75014 Paris, France

⁴ California Institute of Technology, MC 405-47, 1200 E. California Blvd., Pasadena, CA 91125

⁵ Laboratoire d'Astrophysique de Marseille, BP 8, Traverse du Siphon, 13376 Marseille Cedex 12, France

⁶ Center for Space Astrophysics, Yonsei University, Seoul 120-749, Korea ⁷ Space Sciences Laboratory, University of California at Berkeley, 601 Campbell Hall, Berkeley, CA 94720

⁸ Observatories of the Carnegie Institution of Washington, 813 Santa Barbara St., Pasadena, CA 91101

⁹ Laboratory for Astronomy and Solar Physics, NASA Goddard Space Flight Center, Greenbelt, MD 20771

¹⁰ Department of Physics and Astronomy, University of California, Los Angeles, CA 90095

¹¹ Department of Astronomy, Columbia University, New York, NY 10027, USA function papers on GALEX sources and focuses on galaxies at redshifts between z = 0.07 and 0.25. We use photometric redshifts to boost our sample size by a factor of 20 compared to spectroscopic data available. Throughout the paper, we assume a flat Λ CDM cosmology with $\Omega_M = 0.3$ and $H_0 = 70$ km s⁻¹ Mpc⁻¹.

2. THE SAMPLE

The GALEX telescope has two photometric bands at 1530Å (FUV) and 2310Å (NUV) and a 1.2 degree field of view. For a detailed description of survey and performance, see Martin et al. (2004) and Morrissey et al. (2004) in the present volume. Our sample consists of Medium Imaging Survey (MIS) fields overlapping with the Data Release One coverage of the SDSS (DR1; Abazajian et al. 2003), see also Seibert et al. (2004). The depth of the MIS fields is well matched to SDSS and this unique 7-band multicolor dataset provides a good basis for various statistical studies. We select the 57 fields with more than 1400 second exposure times and no objects with higher extinction than E(B-V) = 0.08. We use 36 arcmin radius circles in the center of the fields to ensure uniform image quality. The intersection of the unique area of these MIS fields with the SDSS DR1 footprint is 43.9 square degrees. Our catalog contains only objects that are classified as galaxies by the SDSS photometric pipeline based on their morphology. We use total magnitudes corrected for foreground extinction: SExtractor's MAG_AUTO for GALEX and model magnitudes from SDSS. For the limiting magnitudes, we elect to choose a safe $m_{\text{lim}} = 21.5$ cut in both bands to ensure completeness (Xu et al. 2004).

2.1. Photometric Redshifts

Photometric redshifts are utilized to fully exploit the data set. We choose empirical photometric redshifts over template based estimates because currently the GALEX photometric system is only known to about 10% accuracy and SED fitting is sensitive to zeropoint errors. Following Connolly *et al.*

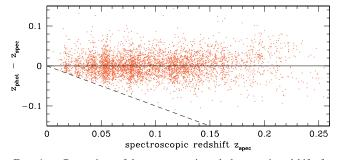


FIG. 1.— Comparison of the spectroscopic and photometric redshifts for the MIS objects in our training set. The equation of the black dashed line is $z_{phot} = 0$.

(1995a), a third order polynomial formula was applied to map the GALEX NUV and SDSS u'g'r'i'z' magnitudes to photometric redshifts. Note that the FUV magnitude was excluded from the fitting formula as the NUV observations go deeper and not all galaxies have FUV measurements. This way there is only one redshift estimator that can be used for both FUV and NUV limited samples. We find that the empirical fit yields reliable redshift estimates out to redshift of 0.25. For the training set of 6295 galaxies, the rms scatter is $\Delta z_{\rm rms} = 0.026$ and there is about 2% outliers. This accuracy is about 15% better than SDSS alone using the same technique. A more detailed analysis and a photometric redshift catalog will be published elsewhere (Budavári et al. 2004c). We expect the uncertainty in the photometric redshifts to be a significant source of error in our statistical analysis, so we adopt a conservative nominal redshift error of $\sigma_z = 0.03$. Figure 1 compares the spectroscopic and photometric redshifts as a function of redshift.

One of the disadvantages of the empirical photometric redshifts is that the method does not provide a direct measurement of the spectral types or K-corrections. To overcome this, we fit synthetic model spectra with full wavelength coverage from the UV to the IR to the SDSS photometry and pick the best fitting template for each galaxy. Our template set has 10 interpolated spectra from Ell to Irr of Bruzual & Charlot (2003). For each of these templates, the K-correction is calculated as a function of redshift. In addition to the galaxy templates, we also include a series of QSO spectra in an attempt to identify AGNs in the sample. Those objects which are best fitted with quasar templates, roughly 10%, are removed from the sample. Our photometric redshift catalog contains 190,489 MIS galaxies out of which 9,356 pass the area, magnitude, redshift and SED cuts in the NUV and 6,174 in FUV.

3. LUMINOSITY FUNCTION RESULTS

There are several methods for calculating the luminosity function (Schmidt 1968; Lynden-Bell 1971; Choloniewski 1986; SubbaRao *et al.* 1996). We use the V_{max} method (Schmidt 1968) to calculate the LF in 0.1 magnitude wide bins, First, we derive the absolute magnitude using the distance modulus and the K-correction, then the maximum redshift where the object could be observed from. The LF is then calculated as $\phi(M) dM = \sum 1/V(z_{\text{max}})$, where $V(z) = \frac{\Omega}{3} d^3(z)$ for a flat universe, Ω is the areal coverage and d(z) is the comoving distance.

To estimate the uncertainty in the LF, we create 50 Monte-Carlo (MC) realizations of the catalogs drawing the redshifts randomly from Gaussian distributions with means of the originally estimated redshifts and widths of $\sigma_z = 0.03$. We coadd the MC realizations for a more robust estimate of the true LF. This method allows us to propagate the errors. The errorbars plotted in the figures are combinations of the variations among the MC realizations and the Poisson errors added in quadrature.

3.1. Evolution with Redshift and Spectral Type

To study the evolution of the UV LF as a function of redshift, we split the sample into three redshift shells. These low, medium and high redshift subsamples have galaxies in the 0.07-0.13, 0.13-0.19 and 0.19-0.25 intervals. Figure 2 shows the FUV and NUV LFs for the three redshift slices along with their best fitting Schechter (1976) functions. The absolute magnitude range over the luminosity functions can be fitted is limited at the faint end by the lower redshift cutoff in the more distance shells and also at the bright end at $M \lesssim -20$, where the measurements depart from the Schechter function. The latter is due to residual contamination from QSO light that the SED fitting could not eliminate completely. The insets show the 1σ , 2σ and 3σ confidence regions on the $M^* - \alpha$ plane. As seen in Figure 2, there is a modest evolution in M^* with redshift in both bands but the leverage is not enough to constrain α to high accuracy at higher redshifts. In all cases, the slope is consistent with $\alpha = -1.1$. Table 1 lists the Schechter parameters.

We further divide the lowest redshift NUV and FUV limited samples into two spectral classes based on the assigned SEDs. The early type galaxy class consists of objects with the five reddest templates and late type galaxies with the five bluer SEDs, which corresponds to a restframe color cut of $(u'-r')_0 = 1.7$. This technique is expected to be more robust than the actual $(u'-r')_0$ discriminator as all multicolor information is used. Figure 3 shows the FUV and NUV luminosity function for the early and late type galaxies. We find that M^* is brighter for the red population by approximately 0.2 magnitudes in FUV and by 0.4 in NUV and α is shallower than for the blue population by 0.3, see Table 1. The marginalized errors on both M^* and α are large but the difference between the joint distribution of parameters is significant (see insets of Figure 3.) When using the restframe colors to split galaxies into red and blue, the plots exhibit the same features; the LFs at the faint end $(M \gtrsim -18)$ are essentially indistinguishable and the bright end is also consistent with the template based results although the difference is slightly less pronounced as expected due to the larger scatter. The inverse concentration indices, simply the ratios of the radii containing 50% and 90% of the Petrosian r' fluxes, scatter significantly but on average they are larger for galaxies in the blue class than the red ones, $C_{\text{blue}}^{-1} = 0.46$ and $C_{\text{red}}^{-1} = 0.42$. The red value is noticeably higher than that of the elliptical SDSS galaxies, $C^{-1} \approx 0.35$ (Strateva et al. 2001), which indicates that our redder class too contains spiral galaxies.

3.2. Luminosity Density

We derive the mean luminosity density (LD) by integrating the luminosity with the Schechter function, $\rho_L = \int \phi(L)LdL = \phi^* L^* \Gamma(\alpha+2)$. In fact, the integral is calculated for not just the optimal fit but over the whole range of parameters. Weighting the results by the probability, $w = \exp(-\chi^2/2)$, is essentially the same as using Monte-Carlo realizations for estimating the errors, $\delta \rho_L^2 = \langle \rho_L^2 \rangle_w - \langle \rho_L \rangle_w^2$. Since the redshift range is limited, the errorbars on the higher redshift bins are rather large. Table 1 shows the LD measurements along with the statistical errors and estimates for the systematics due to cosmic variance

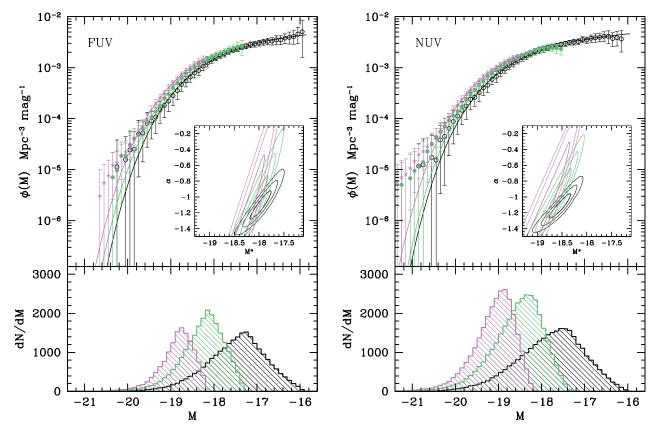


FIG. 2.— The GALEX *FUV* and *NUV* luminosity functions in three redshift bins (*black open circle:* 0.07 < z < 0.13, *green solid circle:* 0.13 < z < 0.19, *magenta star:* 0.19 < z < 0.25.) The top panel illustrates the $1/V_{max}$ measurements along with the best fit Schechter functions. The confidence regions on M^* and α are shown in the insets. The bottom panel shows the number of objects involved in the analysis for a particular selection.

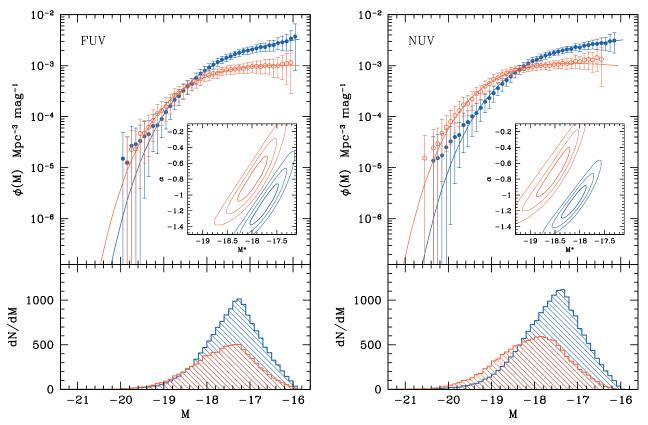


FIG. 3.— The luminosity functions differ in both passbands for the early and late type galaxies in the lowest redshift shell. The red galaxy population is brighter and has a shallower faint-end slope than the blue.

Passband	Redshift	Туре	M^*	α	$\lg \phi^*$ [Mpc ⁻³]	$\lg \rho_L \left[\frac{\operatorname{ergs}}{\operatorname{s}\operatorname{Hz}\operatorname{Mpc}^3}\right]$
<i>FUV</i>	0.07-0.13 0.13-0.19 0.19-0.25	all 	-17.97 ± 0.14 -18.07 ± 0.17 -18.15 ± 0.17	-1.10 ± 0.12 -1.09 ± 0.23 -1.03 ± 0.34	$\begin{array}{c} -2.35 \pm 0.07 \\ -2.33 \pm 0.07 \\ -2.35 \pm 0.06 \end{array}$	$\begin{array}{c} 25.51 \pm 0.02 \pm 0.06 \\ 25.58 \pm 0.07 \pm 0.04 \\ 25.61 \pm 0.12 \pm 0.03 \end{array}$
	0.07–0.13 0.07–0.13	early late	-17.98 ± 0.20 -17.74 ± 0.19	-0.80 ± 0.19 -1.12 ± 0.17	$\begin{array}{c} -2.74 \pm 0.08 \\ -2.47 \pm 0.09 \end{array}$	$\begin{array}{c} 25.06 \pm 0.02 \pm 0.06 \\ 25.31 \pm 0.04 \pm 0.06 \end{array}$
NUV	0.07–0.13 0.13–0.19 0.19–0.25	all 	$\begin{array}{c} -18.54\pm0.15\\ -18.57\pm0.17\\ -18.74\pm0.23\end{array}$	$\begin{array}{c} -1.12\pm 0.10\\ -0.97\pm 0.20\\ -0.99\pm 0.35\end{array}$	$\begin{array}{c} -2.38 \pm 0.07 \\ -2.33 \pm 0.07 \\ -2.39 \pm 0.08 \end{array}$	$\begin{array}{c} 25.71 \pm 0.02 \pm 0.06 \\ 25.74 \pm 0.05 \pm 0.04 \\ 25.79 \pm 0.10 \pm 0.03 \end{array}$
	0.07–0.13 0.07–0.13	early late	-18.53 ± 0.23 -18.11 ± 0.17	-0.73 ± 0.21 -1.09 ± 0.14	-2.66 ± 0.08 -2.48 ± 0.08	$25.35 \pm 0.03 \pm 0.06 \\ 25.43 \pm 0.03 \pm 0.06$

 TABLE 1

 Schechter parameters and luminosity density

that were derived similarly as in Wyder *et al.* (2004). As seen in Figure 4, both ρ_{FUV} and ρ_{NUV} increase with redshift and are consistent with $(1+z)^3$ as well as $(1+z)^{1.5}$. The errorbars in the figure are the combinations of the two sources of errors added in quadrature. They do not include errors from calibration uncertainties of ~10% that may account for $\delta \lg \rho_L = 0.04$ in both bands.

4. DISCUSSION

Using 2dF redshifts, the local GALEX studies by Wyder *et al.* (2004) and Treyer *et al.* (2004) derived very consitent results with the present findings. In the corresponding redshift ranges, the Schechter fits are mostly within the 68% confidence regions with perhaps the one exception of M^* in *NUV*, which seems to be brighter based on this photometric sample. The reason is that the different magnitude cuts in the UV yield slightly different galaxy populations and our sample has more redder galaxies, which makes M^* brighter.

The LD measurements are also in good agreement with Wyder *et al.* (2004), and the observed trend is consistent with the GALEX Deep Imaging Survey results by Arnouts *et al.* (2004) and Schiminovich *et al.* (2004) probing the higher redshift universe out to z = 1.2. The evolution, in turn, is also consistent with results by Wilson *et al.* (2002), who find it to be proportional to $(1+z)^{1.7\pm1.0}$ for galaxies out to z = 1.5 at restframe 2500Å.

Going from the observed UV luminosity function to a SFR function is complicated by dust and the fact that the *FUV* and *NUV* light trace stars forming on different timescales. We will address this problem in subsequent GALEX papers.

- Abazajian, K., et al., 2003, AJ, 126, 2081
- Arnouts, S., et al., 2004, ApJ, present volume
- Bruzual, G., & Charlot, S., 2003, MNRAS, 344, 1000
- Budavári, T., et al., 2004c, in preparation
- Choloniewski, J., 1986, MNRAS, 223, 1
- Connolly, A.J., Csabai, I., Szalay, A.S., Koo, D.C., Kron, R.G., & Munn, J.A., 1995a, AJ, 110, 2655
- Connolly, A.J., Szalay, A.S., Dickinson, M., SubbaRao, M.U., Brunner, R.J., 1997, ApJ, 486, L11
- Cowie, L.L., Songaila, A., Barger, A.J., 1999, AJ, 118, 603
- Kennicutt, R.C., 1998, ARAA&A, 36, 189
- Lilly, S.J., et al., 1996, ApJ, 460, L1
- Lynden-Bell, D., 1971, MNRAS, 155, 95
- Madau, P., 1996, MNRAS, 283, 1388
- Martin, D. C., et al., 2004, ApJ, present volume
- Milliard, B., Donas, J., Laget, M., Armand, C. & Vuillemin, A., 1992, A&A, 257, 24

GALEX (Galaxy Evolution Explorer) is a NASA Small Explorer, launched in April 2003. We gratefully acknowledge NASA's support for construction, operation, and science analysis for the GALEX mission, developed in cooperation with the Centre National d'Etudes Spatiales of France and the Korean Ministry of Science and Technology.

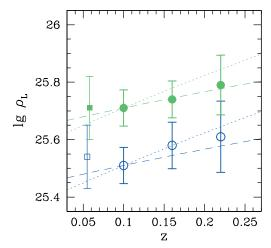


FIG. 4.— The luminosity density as a function of redshift in *FUV* (blue open circles) and *NUV* (green filled circles) along with local GALEX results (squares) by Wyder et al. (2004). The dotted and dashed lines correspond to $(1+z)^3$ and $(1+z)^{1.5}$, respectively, scaled to fit the lowest redshift bin of this study.

REFERENCES

- Morrissey, P., et al., 2004, ApJ, present volume
- Schechter, P., 1976, ApJ, 203, 297
- Schiminovich, D., et al., 2004, ApJ, present volume
- Schmidt, M, 1968, ApJ, 151, 393
- Seibert, M., et al., 2004, ApJ, present volume
- Strateva, I., et al., 2001, AJ, 122, 1861
- SubbaRao, M.U., Connolly, A.J., Szalay, A.S., & Koo, D.C., 1996, ApJ, 112, 929
- Sullivan, M., Treyer, M.A., Ellis, R.S., Bridges, T.J., Milliard, B., & Donas, J., 2000, MNRAS, 312, 442
- Treyer, M.A., et al., 2004, ApJ, present volume
- Wilson, G., Cowie, L.L., Barger, A.J., & Burke, D.J., 2002, AJ, 124, 1258
- Wyder, T.K., et al., 2004, ApJ, present volume
- Xu, K., et al., 2004, ApJ, present volume